

**On the Impact Noise Generation due to a Wheel Passing over  
Rail Joints**

**T.X. Wu and D.J. Thompson**

ISVR Technical Memorandum 863

June 2001



## SCIENTIFIC PUBLICATIONS BY THE ISVR

**Technical Reports** are published to promote timely dissemination of research results by ISVR personnel. This medium permits more detailed presentation than is usually acceptable for scientific journals. Responsibility for both the content and any opinions expressed rests entirely with the author(s).

**Technical Memoranda** are produced to enable the early or preliminary release of information by ISVR personnel where such release is deemed to be appropriate. Information contained in these memoranda may be incomplete, or form part of a continuing programme; this should be borne in mind when using or quoting from these documents.

**Contract Reports** are produced to record the results of scientific work carried out for sponsors, under contract. The ISVR treats these reports as confidential to sponsors and does not make them available for general circulation. Individual sponsors may, however, authorize subsequent release of the material.

## COPYRIGHT NOTICE

(c) ISVR University of Southampton      All rights reserved.

ISVR authorises you to view and download the Materials at this Web site ("Site") only for your personal, non-commercial use. This authorization is not a transfer of title in the Materials and copies of the Materials and is subject to the following restrictions: 1) you must retain, on all copies of the Materials downloaded, all copyright and other proprietary notices contained in the Materials; 2) you may not modify the Materials in any way or reproduce or publicly display, perform, or distribute or otherwise use them for any public or commercial purpose; and 3) you must not transfer the Materials to any other person unless you give them notice of, and they agree to accept, the obligations arising under these terms and conditions of use. You agree to abide by all additional restrictions displayed on the Site as it may be updated from time to time. This Site, including all Materials, is protected by worldwide copyright laws and treaty provisions. You agree to comply with all copyright laws worldwide in your use of this Site and to prevent any unauthorised copying of the Materials.

UNIVERSITY OF SOUTHAMPTON  
INSTITUTE OF SOUND AND VIBRATION RESEARCH  
DYNAMICS GROUP

**On the Impact Noise Generation due to  
a Wheel Passing over Rail Joints**

by

**T.X. Wu and D.J. Thompson**

ISVR Technical Memorandum No: 863

June 2001



## ABSTRACT

Impacts occur when a railway wheel encounters discontinuities such as rail joints. Large impact forces may cause loss of contact between the wheel and rail and damage to the wheel, track and vehicle. Moreover, the consequent impact noise considerably increases the noise from wheel and rail. A model is presented in which the wheel/rail impacts due to rail joints are simulated in the time domain. The impact forces are transformed into the frequency domain and converted into the form of an equivalent roughness input. Using TWINS (Track-Wheel Interaction Noise Software) and the equivalent roughness input, the impact noise radiation is predicted for different rail joints and at various train speeds. It is found that the impact noise radiation due to rail joints is related to the train speed, the joint geometry and the static wheel load. The overall impact noise level from a single rail joint increases with the speed  $V$  at a rate of roughly  $20 \log_{10} V$ . For a jointed track, with joints at fixed distances along the track, the equivalent continuous level due to impact noise increases at  $30 \log_{10} V$  and is found to be 0 - 10 dB higher than the rolling noise due to tread-braked roughness for the joint geometries considered. For undipped or shallow dipped joints the step height is most important in determining the noise level, whereas for more severely dipped joints the effect of the dip is more important than that of the step. For practical rail joints, the gap width has no influence on the noise.



## CONTENTS

1. INTRODUCTION .....	1
2. RAIL JOINT EXCITATION .....	2
3. SIMULATION OF WHEEL/RAIL IMPACT .....	4
4. WHEEL/RAIL IMPACT FORCE .....	6
5. WHEEL AND TRACK RADIATION .....	8
6. CONCLUSIONS .....	11
7. ACKNOWLEDGEMENTS .....	12
REFERENCES .....	13
TABLE .....	14
FIGURES .....	15
APPENDIX A .....	27
APPENDIX B .....	29





## 1. INTRODUCTION

The rail running surface is not perfectly smooth but contains discontinuities, the most severe of which are rail joints. Although continuously welded rail has been widely introduced since the 1960s and 1970s, many rail joints remain on secondary routes, and at points, crossings and track-circuit breaks. The geometry of a rail joint can be characterised by the gap width and the height difference between the two sides of a gap. The gap width may be typically 5-20 mm and the height difference 0-2 mm. In addition the rail often dips near a joint by several millimetres. Even welded rail often has such dipped joints. These discontinuities on the rail can generate large impact forces between the wheel and rail when wheels roll over a dipped rail joint. As a consequence, a transient impact noise is produced in addition to the usual rolling noise, which is more stationary in character.

A comprehensive study was carried out by V  r, Ventres and Myles [1] on estimating impact noise generation due to wheel and rail discontinuities. They developed simple formulae for the speed dependence of the sound power level for three types of rail joint, although the rail joints studied in [1] are flat joints (without dips). Remington [2] extended this work and estimated equivalent roughness spectra corresponding to wheel flats and rail joints. This allowed comparisons of the equivalent spectrum with roughness spectra measured on wheels and rails without significant defects in terms of their noise generation capability. In a different approach, Andersson and Dahlberg [3] studied the wheel/rail impacts at a railway turnout using a finite element model with a moving vehicle. Such a model is rather cumbersome, requiring a time domain solution with many degrees of freedom.

The aim of this report is to explore impact noise generation due to different types of rail joint using an efficient model. Equivalent relative displacement excitations between the wheel and rail are determined from the wheel/rail contact geometry when a wheel rolls over different rail joints. A simplified track model is developed and combined with the wheel through a non-linear Hertzian contact stiffness, to form a wheel/rail interaction model which allows for the possibility of loss of contact between the wheel and rail. Wheel/rail interactions are simulated in the time domain using this model. The resulting impact forces are then transformed into the frequency domain and converted into the form of equivalent roughness spectra. The equivalent roughness spectrum is used as a relative displacement excitation to an established linear wheel/rail interaction model, contained in TWINS (Track-Wheel Interaction Noise Software [4]). Using TWINS, the noise radiation from both wheel and track is predicted for different rail joints and at various train speeds.

## 2. RAIL JOINT EXCITATION

The geometry of a rail joint can be characterised by the width of the gap between the rails and the height difference between the two sides of the gap. The gap width may be typically 5-20 mm and the height difference usually is in a range of 0-2 mm. In addition to the gap and height difference, the rail often dips near a joint because of the way in which rails are manufactured in lengths at the rolling mill. The curve of a dipped rail near the joint can be approximated by quadratic functions. Figure 1 shows the measured profiles of two dipped rail joints. An approximate curve is shown based a quadratic function on either side of the joint. The first joint is approximated quite well, whereas the right-hand side of the second joint differs from the curve. For simplicity in this report, however, the quadratic function will be used. Based on the curves shown in Figure 1, a dipped rail joint with a gap and height difference can also be described using quadratic functions.

To determine the relative displacement input between the wheel and rail, considered as elastic bodies, the trajectory of the centre of a rigid wheel rolling over the rail joint on a rigid track is required [5]. When a wheel rolls on a dipped rail, the wheel centre trajectory can be determined from the fact that the wheel and the rail share a common tangent at the contact point. At a joint, however, the wheel/rail contact geometry may be much more complicated. Figure 2 shows a wheel rolling over a dipped rail joint with a gap and height difference. Three possible situations of wheel/rail contact are shown in Figure 2. They are determined by the geometry of the wheel and the rail joint.

Situation (a) occurs when the gap is not very wide and the dip at the joint is relatively deep. In this situation the wheel and rail are always tangentially in contact. The position at which the wheel is in contact with both rails on the two sides of the joint can be determined according to the contact geometry. Referring to Figure 2(a), the wheel centre trajectory  $z_o, x_o$  can be given as

$$z_o = z_{ri} + r \sin \theta_i, \quad (1a, 1b)$$

$$x_o = x_{ri} + r(1 - \cos \theta_i),$$

$$\theta_i \approx \tan \theta_i = x'_{ri}(z_{ri}), \quad i = 1, 2. \quad (1c)$$

where  $z_{ri}, x_{ri}$  represent the dipped rail curves,  $r$  is the wheel radius and  $'$  indicates the derivative with respect to  $z$ .

Situation (b) occurs when the dip and gap at a joint are small and the height difference between the two sides of the joint is relatively large. There is a position of the wheel such that

it is tangentially in contact with the lower rail (on the left-hand side in Figure 2(b)), but not tangentially in contact with the other rail (the higher rail on the right-hand side), as shown in Figure 2(b). This position can be determined according to the contact geometry. From this position the wheel will pivot about the contact point with the higher rail until the wheel is tangentially in contact with the rail. The wheel centre trajectory in this transitional stage can be calculated using the following formula:

$$\begin{aligned} z_o &= z_R - r \sin \theta, \\ x_o &= x_R + r(1 - \cos \theta), \end{aligned} \quad (2a, 2b)$$

where  $\theta_S - \theta_L \geq \theta \geq \theta_R$  and  $\theta_S$ ,  $\theta_L$  and  $\theta_R$  can be determined according to the wheel radius and the rail joint geometry, see Figure 2(b).

Situation (c) is for a wide gap at the joint which rarely appears in practice. This corresponds, for example, to a gap greater than 20 mm for a 5 mm dipped joint or a gap greater than 35 mm for a 10 mm dipped joint, both without height difference. The wheel centre trajectory in the stage of non tangential contact can be given as follows, refer to Figure 2(c):

$$\begin{aligned} z_o &= z_L + r \sin \theta_1, \\ x_o &= x_L + r(1 - \cos \theta_1), \end{aligned} \quad \text{for } \theta_L \leq \theta_1 \leq \theta_S/2 - \delta, \quad (3a, 3b)$$

$$\begin{aligned} z_o &= z_R - r \sin \theta_2, \\ x_o &= x_R + r(1 - \cos \theta_2), \end{aligned} \quad \text{for } \theta_S/2 + \delta \geq \theta_2 \geq \theta_R, \quad (3c, 3d)$$

where  $\delta = \tan^{-1}(h/w)$ ,  $h$  is the height difference and  $w$  is the gap width.

Because of the motion of the wheel centre described in equations (1-3), an extra vertical inertia force is generated when the wheel rolls on the rail with joints. This inertia force is related to the unsprung mass attached to the wheel axle and also depends on the train speed. As neither the track nor the wheel are rigid, the actual motion of the wheel centre is, of course, much more complicated than as described in equations (1-3). Nevertheless, equations (1-3) can be used as the relative displacement excitation between a flexible track and wheel in the wheel/rail interaction model introduced in the following section.

In Figure 2 all the rails are arranged such that the left-hand side is lower than the right-hand side. This represents a so-called ‘step-up’ joint. For a ‘step-down’ joint the above expressions are still valid but for the opposite direction of the longitudinal position of the wheel centre,  $z_o$ .

Figure 3 shows two examples of the wheel centre trajectory calculations. In both cases the joint gap  $w = 7$  mm and the step-up size  $h = 2$  mm, but the rail dips at the joint are

different, one is 10 mm and the other is 5 mm, in both cases over a length of 1 m. The joint with the 10 mm dip corresponds to situation (a), and that with the 5 mm dip to situation (b). The calculated wheel centre trajectories are very close to the dipped rail curves, especially for the rail with the smaller dip, where a step-up transition from the lower rail to the higher one is rather noticeable in the wheel centre trajectory. From the rail curves and the corresponding wheel centre trajectories in Figure 3 it is found that the gap width of a joint is a less important factor in determining the wheel centre trajectory, compared with the step-up size, provided that the gap width is small, for example less than 20 mm.

A simplified representation of a rail joint is the use of flat rail joints, in which the rails are considered as un-dipped and there is only a gap or/and height difference at the joint. Such rail joints were used by Vér, Ventres and Myles [1]. The contact geometry for a wheel rolling over a flat joint is shown in Figure 4. Figure 4(a) is for a large gap and Figure 4(b) is for a small gap which is the usual case in practice. The wheel centre trajectory in the step-up or step-down stage is given as

$$x_o = \begin{cases} r(1 - \cos \theta_2), & \text{for } h < 0 \text{ (step - down), } 0 \leq \theta_2 \leq \varphi, \\ r(1 - \cos \theta_2) - h, & \text{for } h > 0 \text{ (step - up), } \varphi \geq \theta_2 \geq 0. \end{cases} \quad (4)$$

where  $\varphi = \cos^{-1}(1 - |h|/r)$ .

### 3. SIMULATION OF WHEEL/RAIL IMPACT

As the train speed is much lower than the speed of flexural wave propagation in the rail in the frequency region of interest (50-5000 Hz), a relative displacement excitation model is used to calculate wheel/rail interactions [6]. In such a model the wheel remains stationary on the rail and the wheel centre trajectory  $x_o$  described in equations (1-4) is effectively moved at the train speed between the wheel and rail as a relative displacement excitation [5].

The wheel/track interaction model is shown schematically in Figure 5. The vehicle above the suspension is simplified to a static load  $W$ . The track model is composed of a pair of semi-infinite Timoshenko beams on a continuous spring-mass-spring foundation representing the rail pads, sleepers and ballast respectively. The reason for using semi-infinite beams as an approximation of jointed rails is that the bending stiffness of the rail at a joint is dramatically reduced. Although the rails at a joint are usually connected by a fishplate and can still transmit shear force and bending moment to some extent, for simplicity it is assumed that

a rail joint can only transmit shear force but no bending moment. The dynamic behaviour of a semi-infinite Timoshenko beam on spring-mass-spring foundation is derived in Appendix A. The wheel and rail are connected via a Hertzian contact stiffness which is non-linear; the contact force is proportional to the elastic contact deflection to the power 3/2.

In the relative displacement excitation model the wheel/rail interaction position is chosen to be at the joint of two semi-infinite beams. This leads to the assumption that all the displacement excitation and the wheel/rail interaction are at the joint. In practice, however, the rail dip exists in an extended region to both sides of the joint and the wheel/rail interaction due to the joint also occurs in this region. Thus the use of such a model may introduce some errors. Nevertheless the errors are expected to be small since the differences in the point receptance are small in the vicinity of the joint and the main impact happens quite close to the joint. This will be demonstrated in the following section. Appendix B gives some results of the track receptance for various positions of the forcing point relative to the joint.

Since the contact stiffness is non-linear and loss of contact may occur, it is necessary to calculate the wheel/rail dynamic interaction in the time domain. As both the track and the wheel are assumed to be linear, they can be represented by equivalent systems that have the same frequency response functions. Here the track is approximated by a system with the following frequency response function:

$$H_r(s) = \frac{X(s)}{F(s)} = \frac{b_1 s^3 + b_2 s^2 + b_3 s + b_4}{s^4 + a_1 s^3 + a_2 s^2 + a_3 s + a_4}, \quad (5)$$

where  $X(s)$  and  $F(s)$  are the Laplace transforms of the displacement (output) and the force (input) at the contact position respectively. Constant coefficients  $a_i$  and  $b_i$  are determined by minimising the differences between  $H_r(i\omega)$  and the point receptance of the full track model in the frequency region of interest. This model was first developed by Wu and Thompson [7] for an infinite track. For the track parameters listed in Table 1, the constant coefficients for the jointed track are:

$$\begin{aligned} a_1 &= 1.82 \times 10^3, & a_2 &= 1.33 \times 10^7, & a_3 &= 8.50 \times 10^9, & a_4 &= 4.51 \times 10^{12}, \\ b_1 &= 3.25 \times 10^{-6}, & b_2 &= 3.78 \times 10^{-2}, & b_3 &= 3.28 \times 10^1, & b_4 &= 8.27 \times 10^4, \end{aligned}$$

The wheel is approximated by its unsprung mass,  $M$ , together with a damped spring,  $K$  and  $c$ , giving the following transfer function (receptance):

$$H_w(\omega) = -\frac{K - M\omega^2 + i\omega c}{M\omega^2(K + i\omega c)}. \quad (6)$$

The parameters for the wheel are also listed in Table 1. Comparisons are made in Figure 6 between the approximate models and the full models in terms of the point receptance. Good agreement can be seen for the track models, whereas the high frequency resonances of the wheel are not present in the simplified model. However, the errors caused by using the simplified wheel model can be well compensated using a hybrid model of wheel/rail interaction in the frequency domain [5]. This is discussed in section 5.

The wheel/rail interaction can be determined in the time domain by expressing the equivalent track and wheel models, given by equations (5-6), in a state-space form and coupling them through a Hertzian contact force. This non-linear Hertzian contact force is given as

$$f = \begin{cases} C_H (x_w - x_r - x_o)^{3/2}, & x_w - x_r - x_o > 0, \\ 0, & x_w - x_r - x_o \leq 0, \end{cases} \quad (7)$$

where  $C_H$  is the Hertzian constant,  $x_w$  and  $x_r$  are the displacement of the wheel and rail respectively and  $x_o$  is the relative displacement excitation due to the wheel rolling over the rail joint, described for example in equations (1-4) for the different types of joint. Here  $x_o$  is a function of time and thus becomes dependent upon the train speed.

#### 4. WHEEL/RAIL IMPACT FORCE

Simulations of wheel/rail impact are carried out in the time domain for different types of rail joint and at different train speeds. Figure 7 shows the wheel/rail impact process in the time domain in terms of the contact force and the wheel and rail displacement, for a dipped rail joint with a gap width  $w = 7$  mm and height difference  $h = 1$  mm (step-up) and at speeds 80 and 160 km/h. The dipped rail sections are each chosen to be 0.5 m long each, symmetrical on both sides of the joint as in Figure 1, with the largest dip being 10 mm at the joint. A static force  $W = 100$  kN is applied to represent the vehicle load. When the rail dip appears between the wheel and rail before the joint (the sign convention adopted is positive for a dip and for downwards displacements), the wheel falls and the rail rises, but the wheel cannot immediately follow the dip due to its inertia and thus partial unloading occurs. If the train speed is high, for example at 160 km/h, the static load cannot maintain contact between the wheel and rail and so loss of contact occurs. Impact occurs when the wheel rolls onto the other section of the dipped rail after passing the joint. Here the contact force rises

dramatically and the ratio of the peak force to the static load reaches 4 and 6 for 80 and 160 km/h respectively. Since the momentum of the wheel and rail are changed dramatically by the large impulse during the impact, the wheel and rail are forced to move apart from each other and a second (first, for 80 km/h) loss of contact occurs. Then a second but smaller impact occurs when the wheel hits the rail again. If the train speed is low, loss of contact may not appear between the wheel and rail, but a larger transient force still occurs though with a smaller peak.

The results in Figure 7 illustrate that the impact force caused by rail joints is related to the train speed. The ratio of the peak to static force at different speeds is presented in Figure 8 for different types of rail joint. The rail dip at the joint is assumed to be 5 or 10 mm and in each case 1 m long. In general, the maximum impact force increases as the speed goes up, but the rate of increase becomes smaller for the step-down joints, especially for the rail with the larger dip (10 mm) at speeds over 140 km/h. This can be related to the loss of contact before the impact, seen in Figure 7 for 160 km/h. For the rail with a 5 mm dip, the peak force becomes larger and larger as the step-up size increases from 0 to 3 mm. On the other hand, for the 10 mm dipped rail, the peak force shows only very slight changes when the step-up size varies. Moreover, variations in the peak force with the speed are very similar for both step-up and step-down joints for the 10 mm dipped rail. This indicates that the height differences in the two sides of a rail joint affect the wheel/rail impact more significantly for the lightly dipped rail than for the deeply dipped rail.

Figure 9 shows the results from the flat rail joints (see Figure 4), in which the relative displacement excitation is calculated using equation (4). For the step-up joints the maximum impact force increases with increasing speed, being similar to the 5 mm dipped rail joint. For the step-down joints, however, it only increases slightly as the speed goes up to 50 km/h. After that the maximum impact forces do not increase further and they are almost the same for the three step-down joint sizes considered.

As the wheel and the track are assumed to be linear, their responses to the excitation force can be calculated in the frequency domain. It is useful to transfer the impact force from the time domain to the frequency domain. A Fourier transform is taken of a signal of length 0.125 s and the results are converted into 1/3 octave bands. Note, from Figure 7, that even where there is a step up or down in the rail, the force returns to its initial static value by the end of the time window so there are no truncation errors associated with the Fourier transform.

Figure 10 shows the frequency components of the impact force (during 0.125 second) in 1/3 octave bands due to a wheel passing over different rail joints at various speeds. It can be

seen that the impact force spectrum generally decreases with increasing frequency. The spectra all have a similar shape. The local peaks at about 240 Hz and the local troughs at about 550 Hz in the force spectra correspond to the trough at 240 Hz and the peak at 550 Hz in the point receptance of the track, refer to Figure 6. The force spectrum can be seen to increase with increasing train speed.

## 5. WHEEL AND TRACK RADIATION

The responses of the wheel and track to the impact force are calculated in the frequency domain. Suitable models for the prediction of structural response and sound radiation of wheels and tracks are available within the TWINS model [4] which is used for predicting rolling noise due to random roughness excitation. These models operate in the frequency domain and are normally used with a linear interaction model (linear contact stiffness and no loss of contact allowed between the wheel and rail). For a roughness excitation  $R(\omega)$  at angular frequency  $\omega$ , and considering only interaction in the vertical direction, the interaction force  $F(\omega)$  is given by

$$F(\omega) = -\frac{R(\omega)}{\alpha^W(\omega) + \alpha^C(\omega) + \alpha^R(\omega)}, \quad (8)$$

where  $\alpha^W$ ,  $\alpha^C$  and  $\alpha^R$  are the receptances of the wheel, the contact spring and the rail respectively.

In order to use TWINS to predict impact noise due to rail joints, the impact force in the time domain must be transformed into the frequency domain and the force spectrum must be converted back to ‘an equivalent roughness spectrum’ — the roughness (relative displacement) input between the wheel and rail models that would produce the same force spectrum if the contact spring were linear and there was no loss of contact between the wheel and rail. This is done by using equation (8) in reverse:

$$R_{eq}(\omega) = -F(\omega)(\alpha^W(\omega) + \alpha^C(\omega) + \alpha^R(\omega)), \quad (9)$$

where  $F(\omega)$  is the impact force spectrum,  $\alpha^W$  and  $\alpha^R$  correspond to the models used in the time domain calculation and  $\alpha^C$ , the receptance of the contact spring, is from a linear contact spring equivalent to the non-linear Hertzian contact stiffness. The equivalent roughness spectra corresponding to the impact forces due to a wheel passing over rail joints then can be used as inputs into TWINS to predict noise radiation from the wheel and track.



It is known from studies of rolling noise that the wheel modes containing a significant radial component of motion at the contact zone dominate the noise radiation of the wheel/rail system in the frequency region above about 2 kHz [8]. In TWINS, the wheel is therefore represented by its full modal basis in the frequency range up to 6 kHz. This is determined from a finite element model. On the other hand, however, the full modal basis for the wheel is not included in the time domain model of wheel/rail interaction (see the wheel receptance in Figure 6). The question that remains, therefore, is whether the high frequency modes can appropriately be included in the structural response of the wheel by using the equivalent roughness input in TWINS. It has been found in [5] that the high frequency modal behaviour of the wheel can be taken into account quite precisely by this means, even though it is not present in the simplified model and thus excluded from the simulations of the wheel/rail impact in the time domain.

The equivalent roughness spectra derived from equation (9) are now used as inputs to the frequency domain calculations of wheel/rail noise using the TWINS model. The wheel is represented by its full modal basis in the frequency range up to 6 kHz, as mentioned above, and the track is modelled by an infinite Timoshenko beam continuously supported on a spring-mass-spring foundation. The track parameters are listed in Table 1. Wheel/rail interaction is included in both vertical and lateral directions, the excitation being in the vertical direction.

The results from TWINS are then corrected to convert them to the situation modelled, in which the rail is semi-infinite with a pin joint at the excitation point. This correction is made by two factors  $C_1$  and  $C_2$  according to equation (8):

$$C_1 = \frac{F_{semi}}{F_{inf}} = \frac{\alpha^W(\omega) + \alpha^C(\omega) + \alpha_{inf}^R(\omega)}{\alpha^W(\omega) + \alpha^C(\omega) + \alpha_{semi}^R(\omega)}, \quad (10)$$

$$C_2 = \frac{\alpha_{semi}^R(\omega)}{\alpha_{inf}^R(\omega)}, \quad (11)$$

where  $\alpha_{inf}^R(\omega)$  and  $\alpha_{semi}^R(\omega)$  are the point receptance of the infinite beam and semi-infinite beam respectively. The factor  $C_1$  is applied as a correction to the wheel response and the product  $C_1 C_2$  is used for the rail and sleeper responses. These corrections are shown in Figure 11. This shows that the correction applied to the track is close to 0 dB in the region 100 - 1000 Hz, which is where its radiation dominates the total. Conversely, the correction applied to the wheel is close to 0 dB at higher frequencies, where the wheel radiation is the most important component.

Figure 12 shows the equivalent roughness spectra corresponding to the impact force spectra in Figure 10 and the predicted overall sound power radiated by one wheel and the associated track vibration. The sound power represents the radiation emitted during 0.125 s. Results are shown here for dipped rails with a 1 mm step-up joint at various train speeds. The equivalent roughness spectrum can be seen to increase with increasing speed and to reduce with frequency at a rate of approximately  $-30 \log_{10} f$ . The noise radiation shows a more complicated variation with frequency because it comes from three sources, the wheel, rail and sleeper, and they have different dynamic behaviour and radiation properties in the frequency region studied. Nevertheless, the noise increases at all frequencies as the speed increases. For step-down joints the equivalent roughness and the radiation are similar and thus are not shown.

Figure 13 presents a summary of the variation of the overall A-weighted sound power level with train speed for different types of dipped rail joint. As in the previous figures, these results correspond to the average sound pressure during 0.125 s. All the curves show that the noise radiation generally increases with increasing speed, regardless of whether loss of contact occurs. For the lightly dipped rail (5 mm dip at the joint) with a step-up joint, the predicted noise level steadily increases at a rate of approximately  $20 \log_{10} V$ , where  $V$  is the train speed. The rate of increase for a step-down joint is not as high as for a step-up joint. Again for the lightly dipped rail, the noise radiation increases significantly by up to 8 dB when the step-up size increases from 0 to 2 mm, whereas for the more deeply dipped rail (10 mm dip at the joint), it remains almost unchanged when the step-up size increases from 0 to 1 mm, and increases only by at most 3 dB between 1 mm to 2 mm. Moreover, the increase of the noise radiation versus speed is very limited after about 100 km/h for the more deeply dipped rail. The results for the 10 mm dip are similar for both step-up and step-down joints. This indicates that, in this case, the shape of the dipped rail at the joint affects the noise radiation more significantly, whereas for the lightly dipped rail it is the height difference between the two sides of a joint that affects the noise radiation more significantly. A similar conclusion was reached in the last section in terms of the peak impact force. Also shown in Figure 13 is the predicted rolling noise level due to typical roughness on tread-braked wheels and good quality track, which increases at a rate of approximately  $30 \log_{10} V$ .

Figure 14 shows the sound power level due to a wheel passing over a flat rail joint at various speeds. It can be seen that the noise level continuously increases at a rate of approximately  $20 \log_{10} V$  when the wheel steps up the joint. When the wheel steps down the joint, the noise radiation increases very little as the train speed increases.

Figure 15 shows the effect of wheel load. The overall A-weighted sound power level is plotted against train speed for dipped rails with a 1 mm step-up joint at two values of wheel load, 50 kN and 100 kN. This corresponds to the difference between typical passenger vehicles (50 kN) and loaded freight vehicles (100 kN). Greater loss of contact between the wheel and rail occurs for 50 kN than for 100 kN but the peak impact force is lower for the former than for the latter. In addition, the corresponding TWINS calculations include the effect of the change in the contact stiffness. The final effects on the noise radiation are therefore a combination of all the above factors. From Figure 15, the noise level can be seen to increase slightly at the speeds up to 120 km/h as the wheel load is reduced, and to reduce at high speeds (where greater loss of contact occurs) by about 5 dB for the lightly dipped rail joint. The effects of the static load on impact noise generation are thus rather complicated.

In comparing impact noise levels with rolling noise levels, as mentioned before, Figure 13 was based on an averaging time of 0.125 second. This is the averaging time of a sound level meter in the 'fast' setting, and gives an indication of short term perception. However, it is also instructive to compare the contributions of impact noise and rolling noise to equivalent continuous levels. For this, the averaging time needs to be adjusted to the time between two rail joints, which are normally 18 m apart. As this time reduces with increasing speed, it is found that the average noise due to impacts increases at a rate of  $30 \log_{10} V$ , similar to rolling noise. The equivalent noise from the dipped rail joints considered is found to be 0 - 10 dB higher than that from rolling noise, as shown in Figure 16.

## 6. CONCLUSIONS

Impact noise generation due to a wheel passing over rail joints has been studied using an efficient theoretical model. Equivalent relative displacement excitations between the wheel and rail have been determined from the wheel/rail contact geometry at the rail joints. A time-domain wheel/rail interaction model has been developed by combining the simplified track and wheel models via a non-linear contact spring. The resulting impact forces were converted into the form of equivalent roughness spectra in the frequency domain. By using the equivalent roughness as input in the TWINS model, the noise radiation from both wheel and track has been predicted for different rail joints and at various train speeds.

The wheel/rail impact due to a wheel passing over a rail joint and the consequent impact noise radiation from the wheel and track are found to be related to the train speed, the geometry of the rail joint and the static wheel load. As the train speed increases, the overall impact noise level from a single joint increases with the train speed  $V$  at a rate of roughly  $20 \log_{10} V$ . This differs from rolling noise due to roughness excitation which generally increases at  $30 \log_{10} V$ . However, for a jointed track with regularly spaced joints, the contribution of the impact noise to the equivalent continuous level will also increase at  $30 \log_{10} V$ . A large difference in height between the two sides of a step-up joint may generate higher level impact noise for a lightly dipped rail than for a deeply dipped rail. For a lightly dipped rail, a step-down joint usually generates less noise than a step-up joint, whilst for a deeply dipped rail the noise levels are the same for both types of joint. The effects of the static load on impact noise generation are complicated; under smaller static load, greater loss of contact between the wheel and rail may occur and the noise level may increase at lower speeds, but at higher speeds it reduces.

## 7. ACKNOWLEDGEMENTS

The work described has been performed within the project ‘Non-linear Effects at the Wheel/rail Interface and their Influence on Noise Generation’ funded by EPSRC (Engineering and Physical Sciences Research Council of the United Kingdom), grant GR/M82455. The authors are grateful to J. W. Edwards of Infracore BCV (formerly part of London Underground) for supplying dimensions of typical rail joints.

## REFERENCES

1. I. L. VÉR, C. S. VENTRES and M. M. MYLES 1976 *Journal of Sound and Vibration* **46** 395-417. Wheel/rail noise—Part III: Impact noise generation by wheel and rail discontinuities.
2. P. J. REMINGTON 1987 *Journal of Sound and Vibration* **116** 339-353. Wheel/rail squeal and impact noise: What do we know? What don't we know? Where do we go from here?
3. C. ANDERSSON and T. DAHLBERG 1998 *Proceedings of the Institution of Mechanical Engineers Part F* **212** 123-134. Wheel/rail impacts at a railway turnout crossing.
4. D. J. THOMPSON and M. H. A. JANSSENS 1997 *TNO report TPD-HAG-RPT-93-0214*, *TNO Institute of Applied Physics*. TWINS: Track-wheel interaction noise software. Theoretical manual, version 2.4.
5. T. X. WU and D. J. THOMPSON 2001 *ISVR Technical Memorandum* No. 859, *University of Southampton*. A hybrid model for wheel/track dynamic interaction and noise generation due to wheel flats.
6. S. L. GRASSIE, R. W. GREGORY, D. HARRISON and K. L. JOHNSON 1982 *Journal of Mechanical Engineering Science* **24** 77-90. The dynamic response of railway track to high frequency vertical excitation.
7. T. X. WU and D. J. THOMPSON 2000 *Vehicle System Dynamics* **34** 261-282. Theoretical investigation of wheel/rail non-linear interaction due to roughness excitation.
8. D. J. THOMPSON and C. J. C. JONES 2000 *Journal of Sound and Vibration* **231** 519-536. A review of the modelling of wheel/rail noise generation.

TABLE 1

*Parameters of wheel and track*

Wheel mass (all unsprung mass), kg	$M$	600
Modal stiffness, N/m	$K$	$4.59 \times 10^9$
Damping, N·s/m	$c$	$1.66 \times 10^4$
Hertzian constant, $\text{N/m}^{3/2}$	$C_H$	$9.37 \times 10^{10}$
Young's modulus of rail, $\text{N/m}^2$	$E$	$2.1 \times 10^{11}$
Shear modulus of rail, $\text{N/m}^2$	$G$	$0.77 \times 10^{11}$
Density of rail, $\text{kg/m}^3$	$\rho$	7850
Loss factor of rail	$\eta_r$	0.01
Cross-section area of rail, $\text{m}^2$	$A$	$7.69 \times 10^{-3}$
Area moment of inertia, $\text{m}^4$	$I$	$30.55 \times 10^{-6}$
Shear coefficient	$\kappa$	0.4
Pad stiffness, $\text{N/m}^2$	$k_p$	$5.83 \times 10^8$
Pad loss factor	$\eta_p$	0.25
Sleeper mass (half), kg/m	$m_s$	270
Ballast stiffness, $\text{N/m}^2$	$k_b$	$8.33 \times 10^7$
Ballast loss factor	$\eta_b$	1

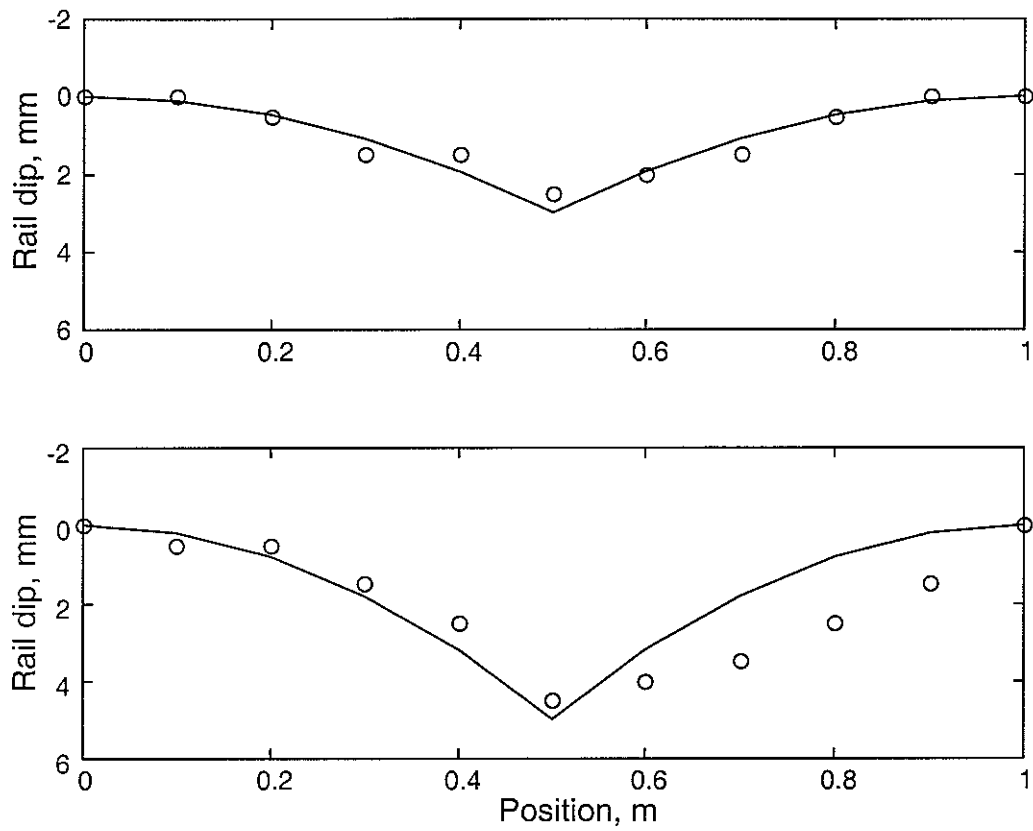


*Fig. 1. Dipped rail shape at two typical joints. —quadratic function, o from measurement.*

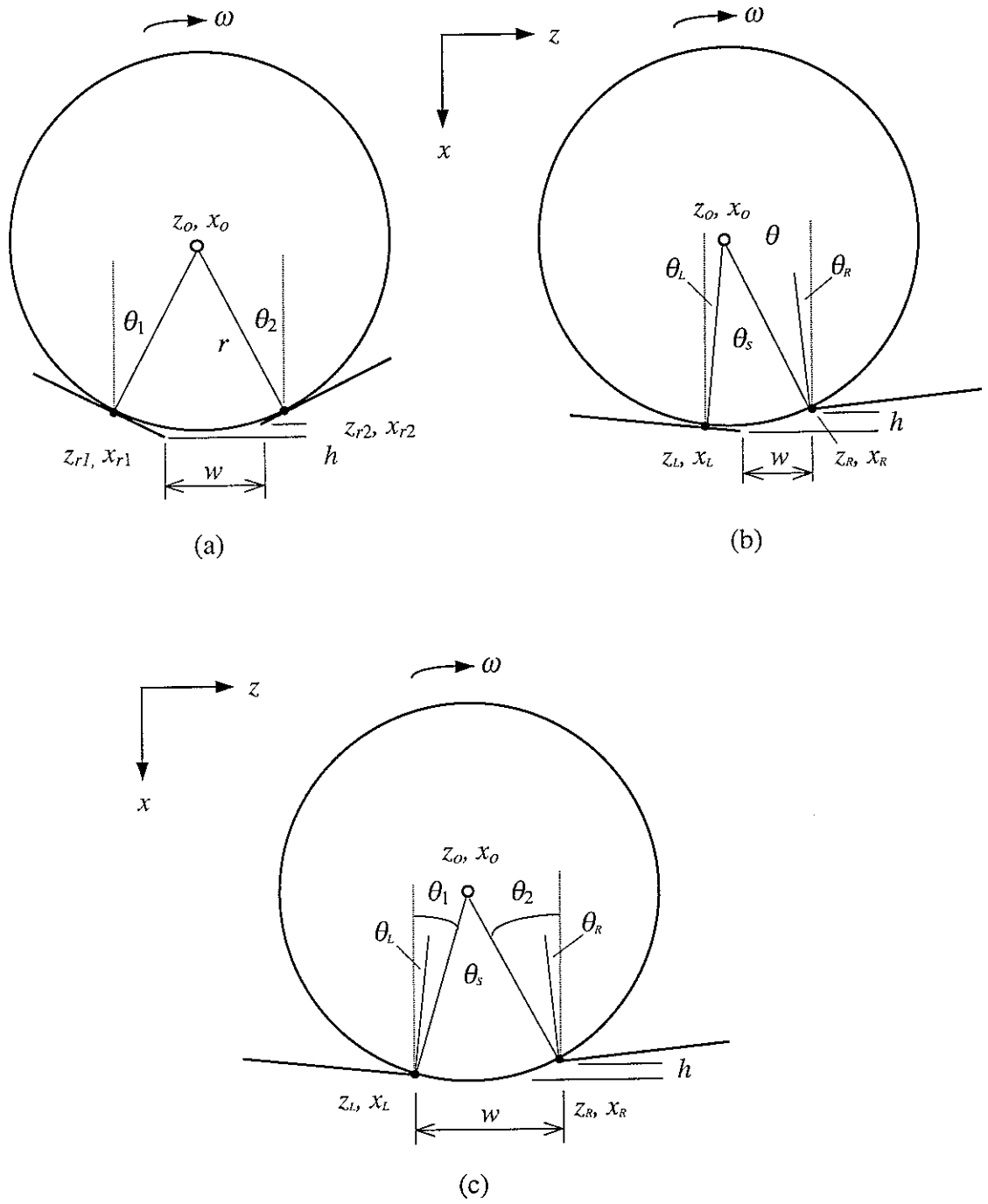


Fig. 2. Rolling contact geometry of a wheel over dipped rails at a joint.



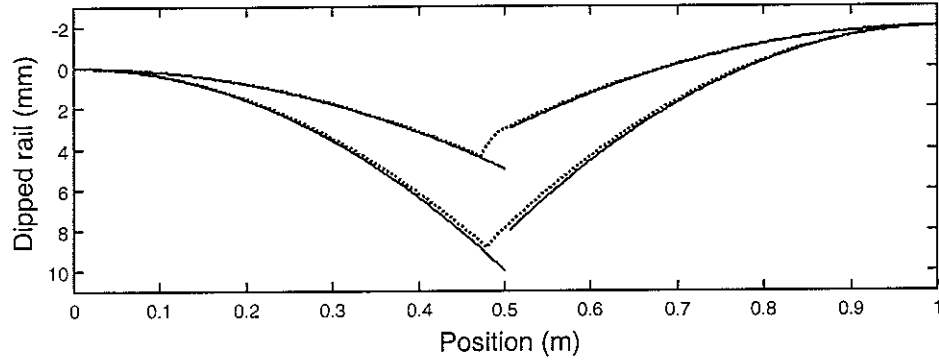


Fig. 3. Wheel centre trajectory for a wheel rolling over a dipped rail joint. — dipped rail shape, ..... wheel centre trajectory. Upper curves are for a 5 mm dip at the joint, bottom curves for a 10 mm dip at the joint.

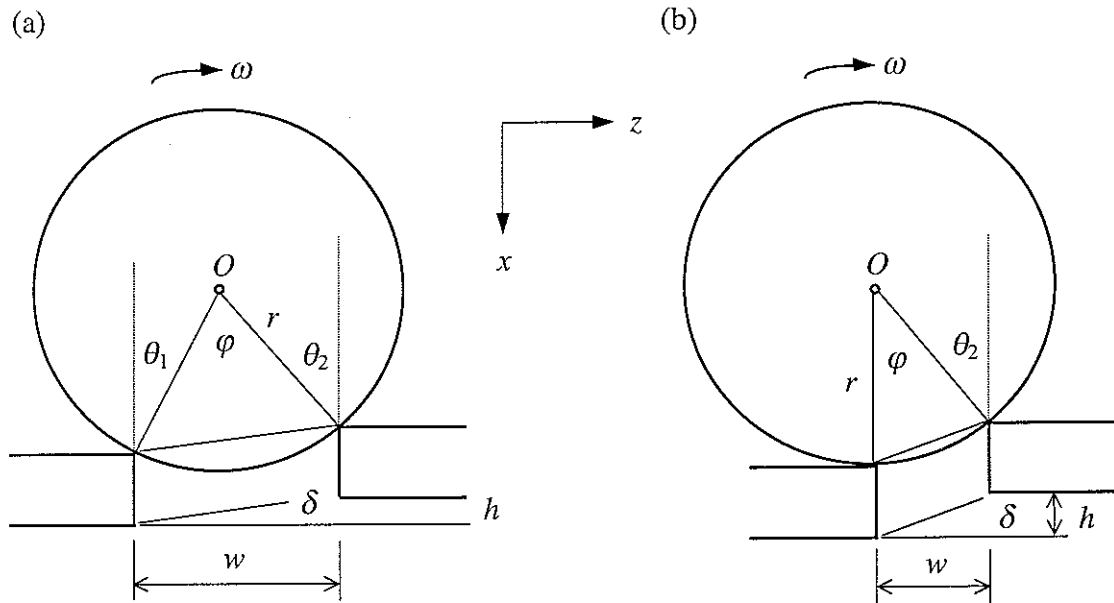
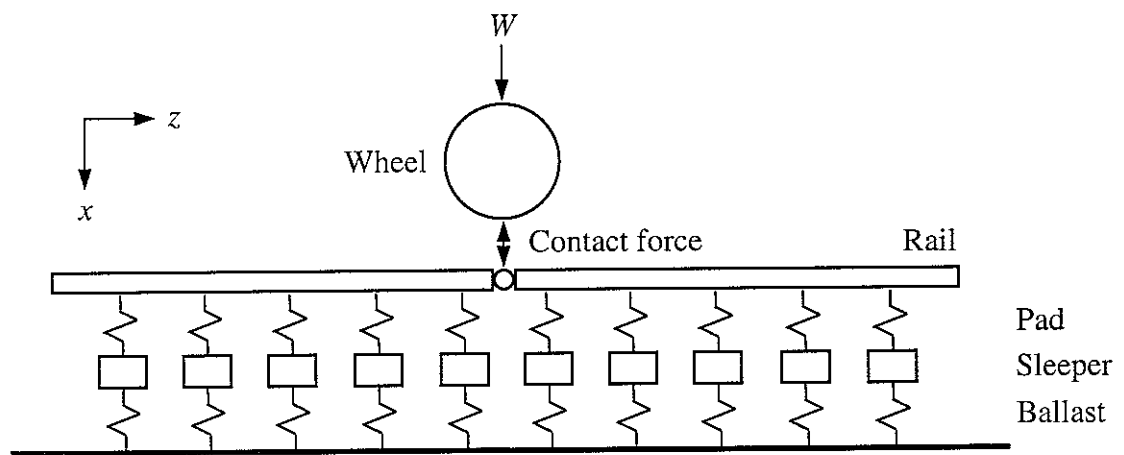


Fig. 4. Rolling of a wheel over a flat rail joint.



*Fig. 5. Wheel/track interaction model at a joint.*

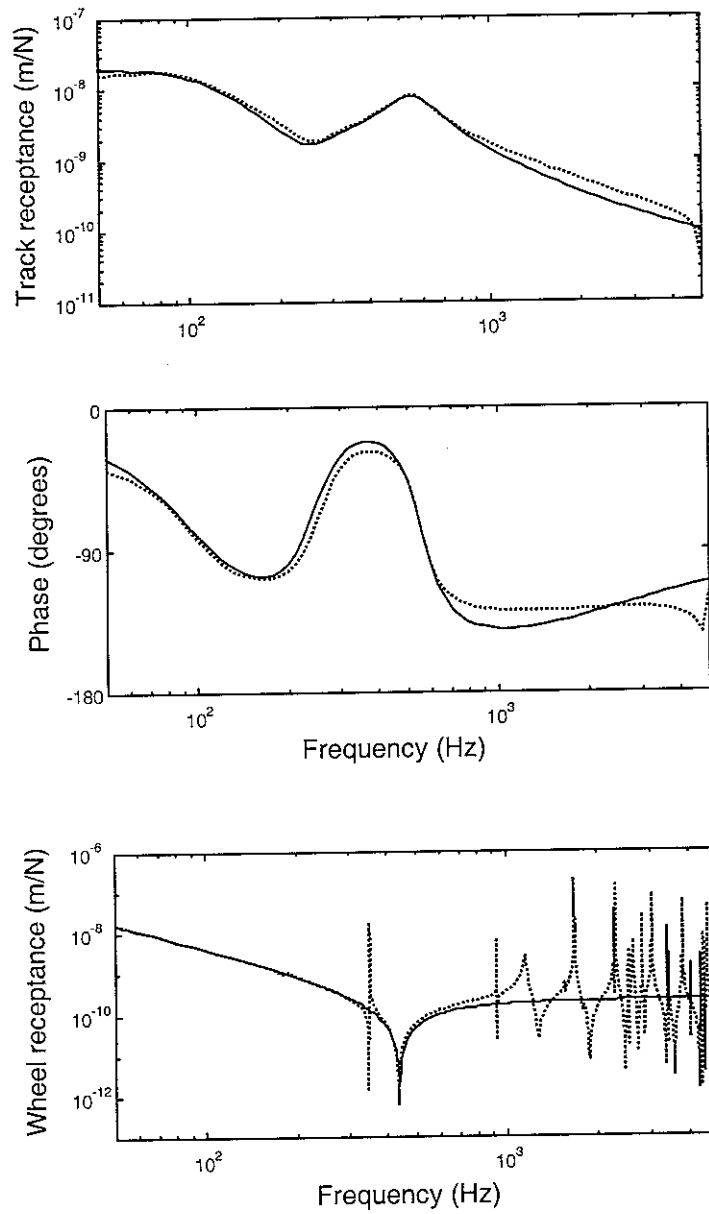


Fig. 6. Track and wheel receptance at contact point. For the track both magnitude and phase are shown and only magnitude is shown for the wheel. — from simplified models, ..... from full models.

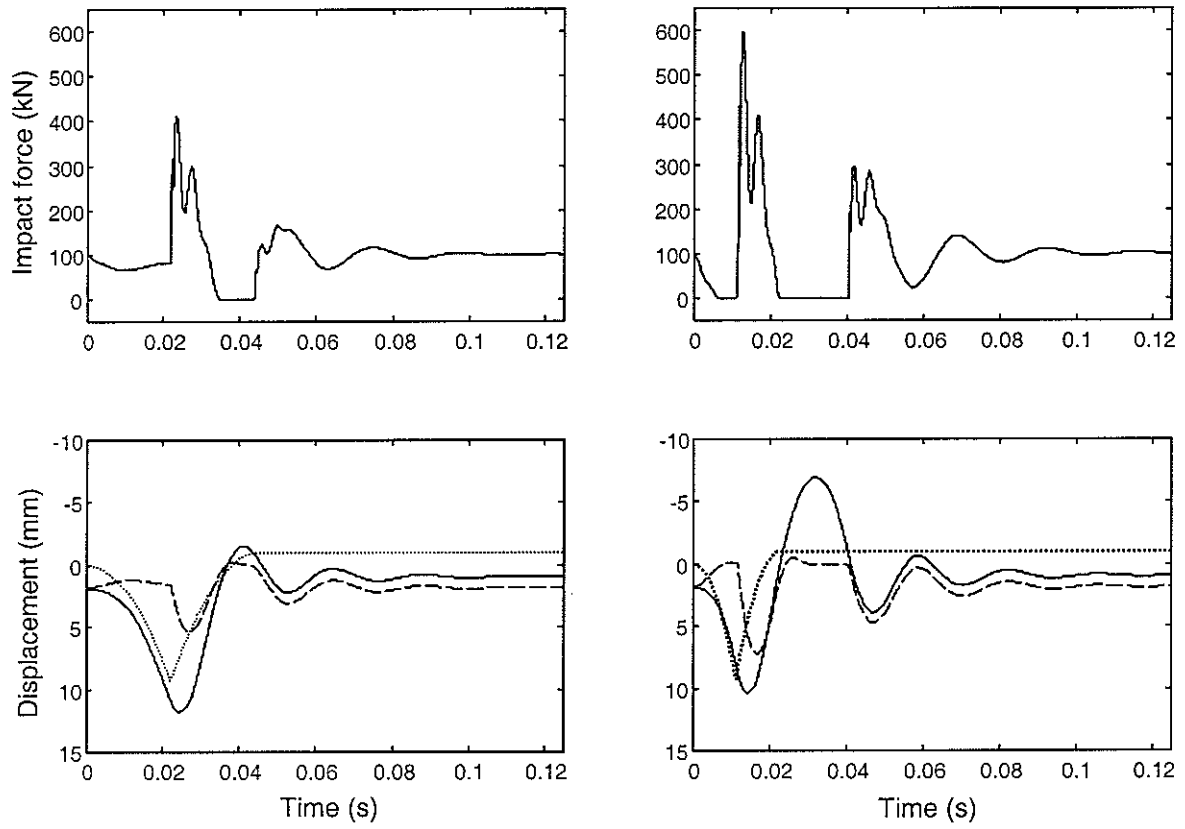


Fig. 7. Wheel/rail impact at a dipped rail joint with a gap  $w = 7$  mm and a step-up  $h = 1$  mm and under a static load  $W = 100$  kN. Left: at 80 km/h, Right: at 160 km/h. — impact force and wheel displacement, - - - rail displacement, ..... wheel centre trajectory (relative displacement excitation).

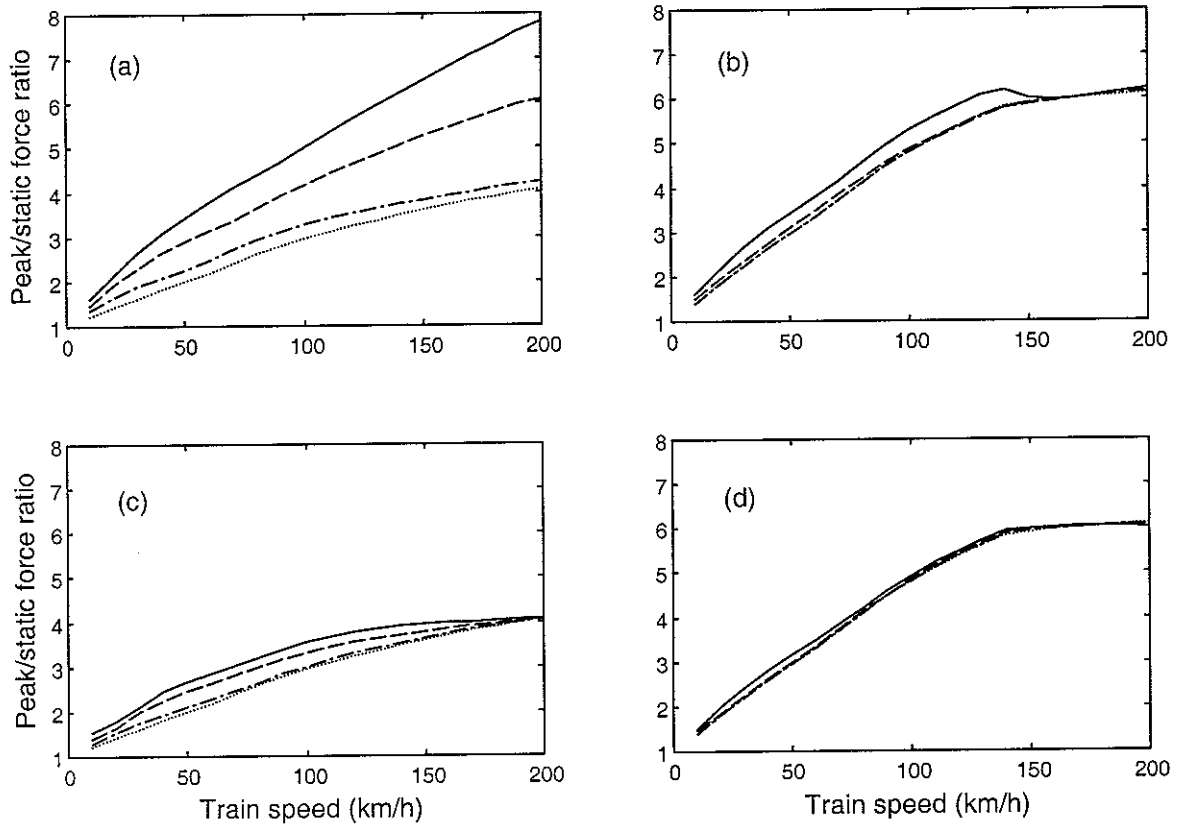


Fig. 8. Ratio of the maximum impact force to the static load. (a) for step-up joints with 7 mm gap and 5 mm dip, (b) for step-up joints with 7 mm gap and 10 mm dip, (c) for step-down joints with 7 mm gap and 5 mm dip, (d) for step-down joints with 7 mm gap and 10 mm dip. .... height difference  $h = 0$ , - · -  $h = 1$  mm, ---  $h = 2$  mm, —  $h = 3$  mm.

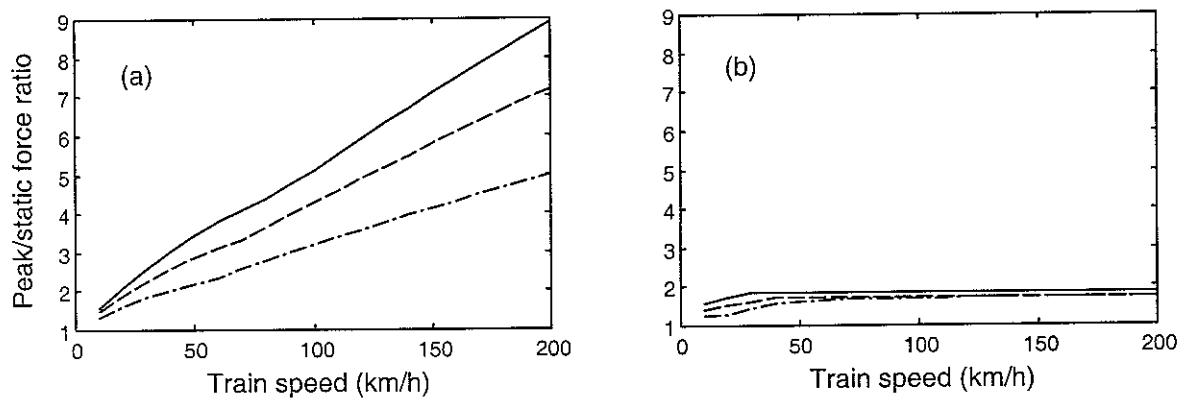


Fig. 9. Ratio of the maximum impact force to the static load for the flat rail joints. (a) for step-up joints, (b) for step-down. , - · - height difference  $h = 1$  mm, ---  $h = 2$  mm, —  $h = 3$  mm.

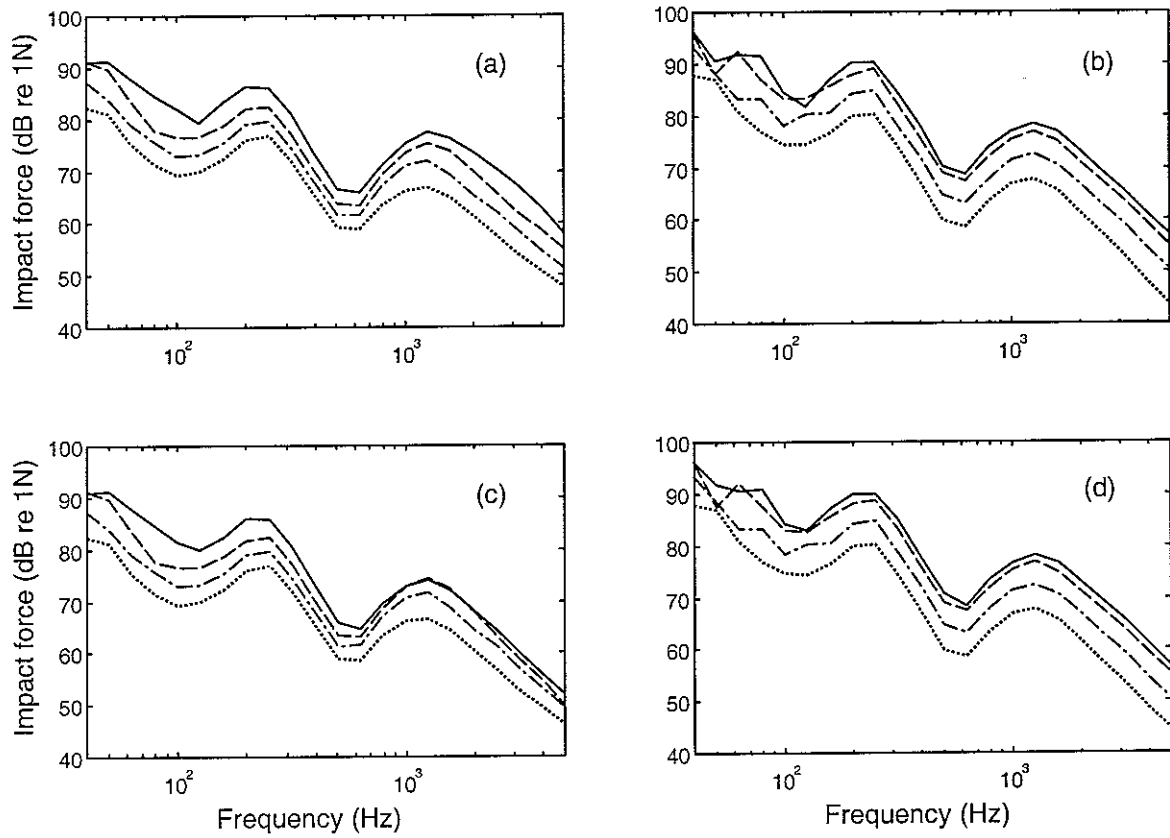


Fig. 10. Impact force spectra in 1/3 octave bands due to a wheel passing over a rail joint with 7 mm gap and 1 mm height difference at various speeds. (a) from a step-up joint with 5 mm dip, (b) from a step-up joint with 10 mm dip, (c) from a step-down joint with 5 mm dip, (d) from a step-down joint with 10 mm dip. ..... 50 km/h, - · - 80 km/h, - - - 120 km/h, — 200 km/h.

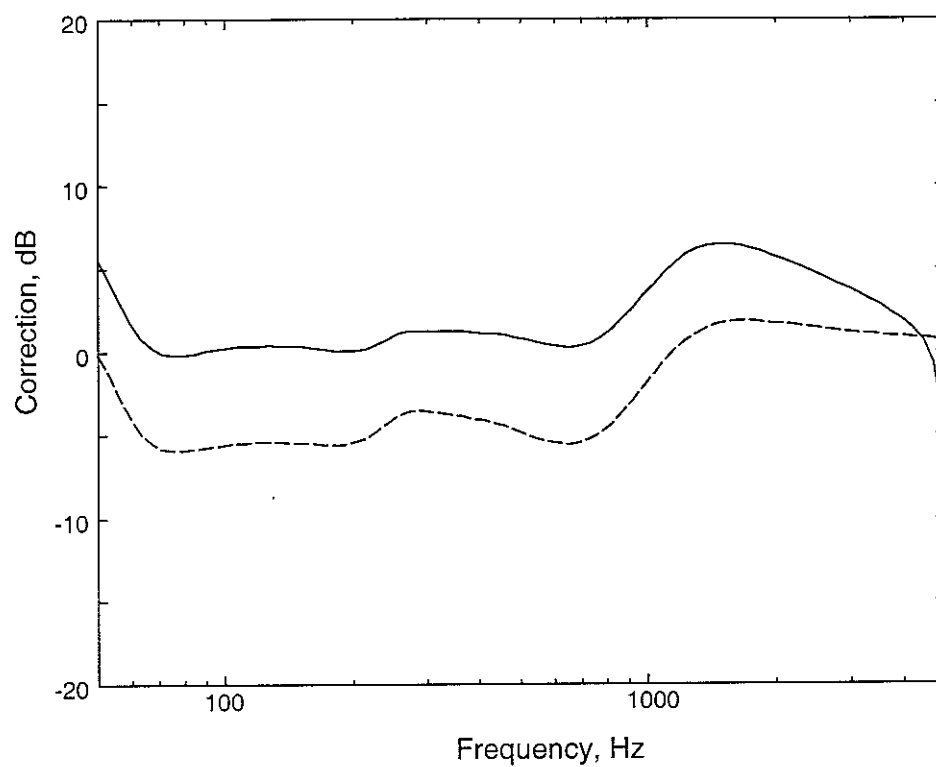


Fig. 11. Corrections applied to TWINS results to convert them from an infinite track to a pin-jointed track. — correction to track noise ( $C_1, C_2$ ), - - - correction to wheel noise ( $C_1$ ).

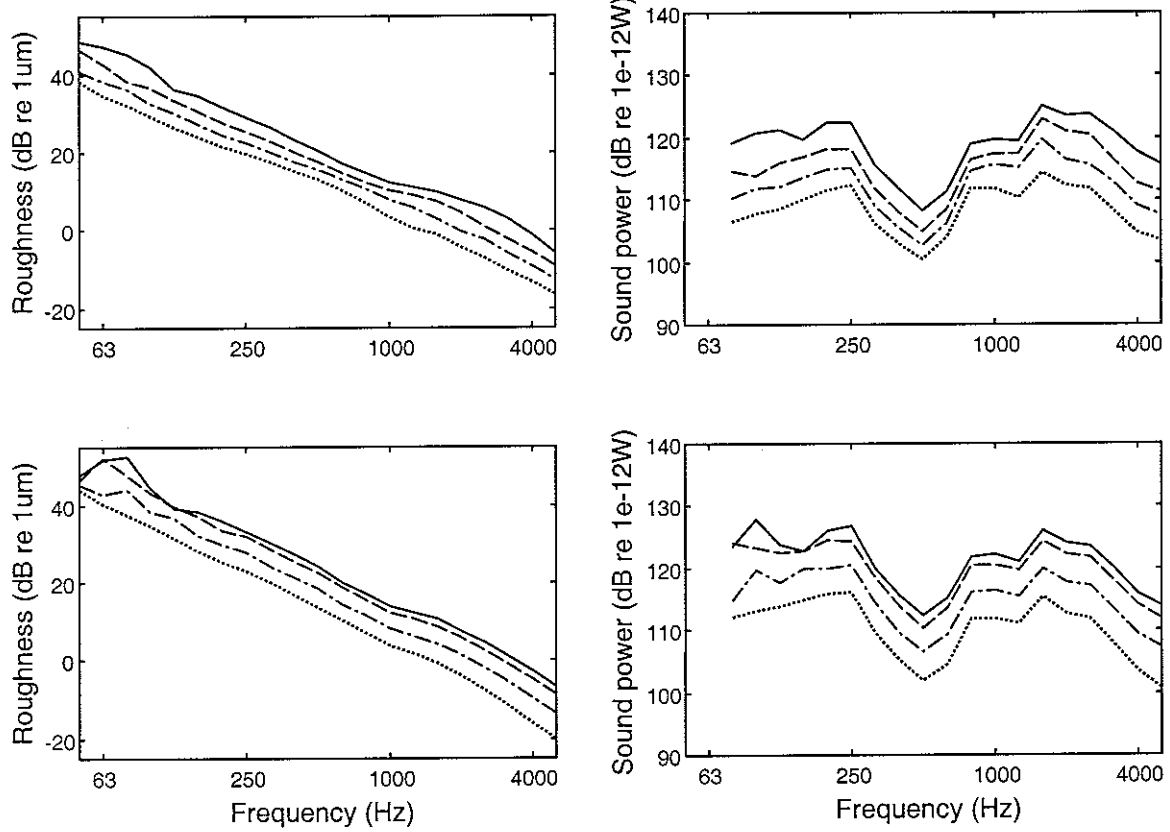


Fig. 12. Equivalent 1/3 octave roughness spectra and sound power levels due to a wheel passing over a rail joint with 7 mm gap and 1 mm step-up at various speeds. Upper: 5 mm dip, Lower: 10 mm dip. .... 50 km/h, - · - · 80 km/h, - - - 120 km/h, — 200 km/h.



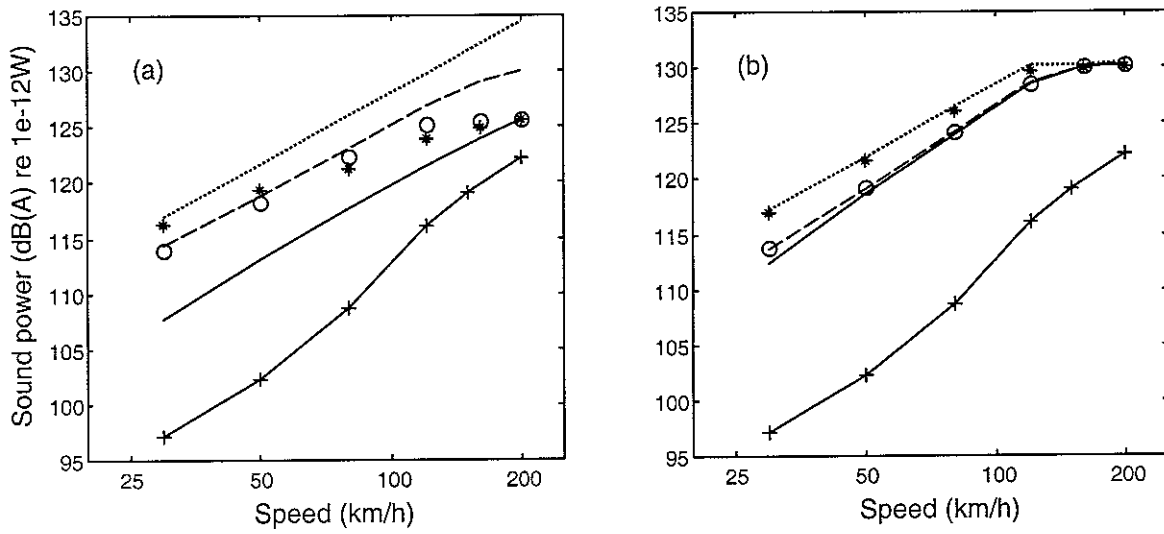


Fig. 13. A-weighted sound power radiated by one wheel and the associated track vibration during 0.125 second due to a wheel passing over different rail joints with 7 mm gap and 5 or 10 mm dip. (a) for 5 mm dip, (b) for 10 mm dip. ..... 2 mm step-up, - - - 1 mm step-up, — no height difference, \* 2 mm step-down, O 1 mm step-down, +—+ rolling noise due to roughness (tread-braked wheel).

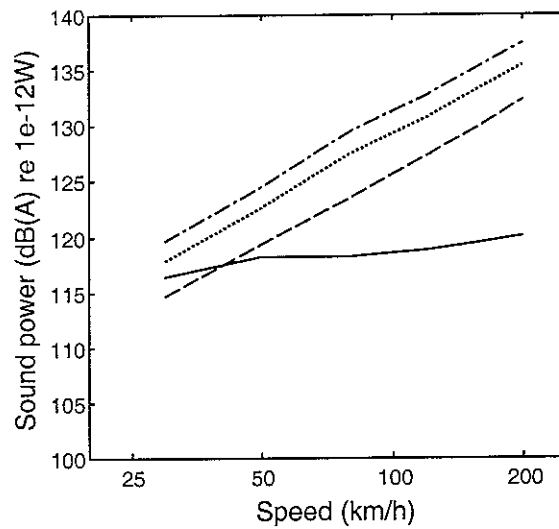


Fig. 14. A-weighted sound radiated by one wheel and the associated track vibration during 0.125 second due to a wheel passing over flat rail joints, - - - 1 mm step-up, ..... 2 mm step-up, ···· 3 mm step-up, — 2 mm step-down.

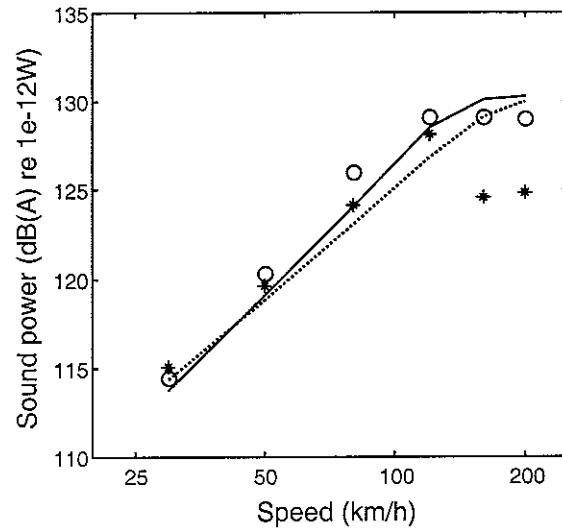


Fig. 15. A-weighted sound power radiated by one wheel and the associated track vibration during 0.125 second due to a wheel passing over a 1 mm step-up joint with 7 mm gap and at two values of wheel load. — 10 mm dip and 100 kN load, ○ 10 mm dip but 50 kN load, ..... 5 mm dip and 100 kN load, \* 5 mm dip but 50 kN load.

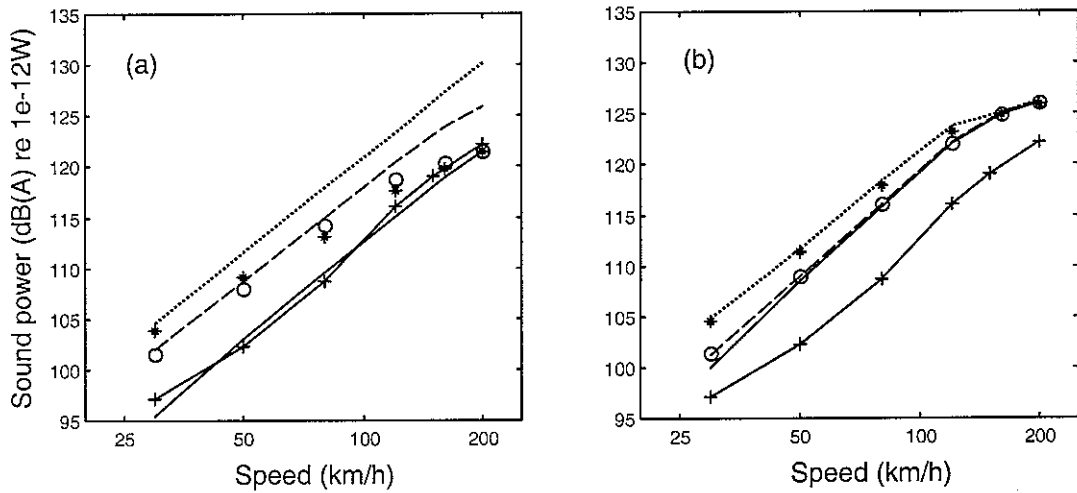


Fig. 16. Equivalent A-weighted sound power radiated by one wheel and the associated track vibration due to wheel/rail impact averaged over a period of 18 m travel. Rail joints with 7 mm gap and 5 or 10 mm dip. (a) for 5 mm dip, (b) for 10 mm dip. ..... 2 mm step-up, - - - 1 mm step-up, — no height difference, \* 2 mm step-down, ○ 1 mm step-down, +—+ rolling noise due to roughness (tread-braked wheel).

# APPENDIX A. RESPONSE TO A HARMONIC FORCE AT THE FREE END OF A SEMI-INFINITE TIMOSHENKO BEAM ON A CONTINUOUS SPRING-MASS-SPRING FOUNDATION

Equations of motion for a Timoshenko beam on a spring-mass-spring layer foundation are

$$-\rho A \omega^2 u + GA \kappa (\phi' - u'') + k_p (u - u_s) = 0, \quad (\text{A1})$$

$$-\rho I \omega^2 \phi + GA \kappa (\phi - u') - EI \phi'' = 0, \quad (\text{A2})$$

$$-m_s \omega^2 u_s - k_p u + (k_p + k_b) u_s = 0, \quad (\text{A3})$$

where  $u$  and  $\phi$  are the vertical displacement and rotation of the cross-section of the beam respectively,  $u_s$  is the displacement of the mass layer, ' indicates the derivative with respect to  $z$ , the longitudinal position of the beam. As both excitation and response are harmonic, the term  $e^{i\omega t}$  is omitted from  $u$ ,  $\phi$  and  $u_s$ .  $E$  is the Young's modulus,  $G$  is the shear modulus and  $\rho$  is the density. The geometric properties of the cross-section are characterised by  $A$ , the cross-sectional area,  $I$ , the area moment of inertia and  $\kappa$ , the shear coefficient. For the foundation  $m_s$  is the mass density per unit length,  $k_p$  and  $k_b$  are the pad and ballast stiffness per unit length respectively. Damping can be added by means of a loss factor to the pad and ballast stiffness to make them complex in the form of  $k(1+i\eta)$ .

Eliminating  $u_s$  from equation (A1) by making use of equation (A3), equation (A1) can be written as

$$-\rho A \omega^2 u + GA \kappa (\phi' - u'') + k_f u = 0, \quad (\text{A4})$$

where  $k_f$  is the dynamic stiffness of the spring-mass-spring layer foundation,

$$k_f = \frac{k_p (k_b - m_s \omega^2)}{k_p + k_b - m_s \omega^2}. \quad (\text{A5})$$

The external excitation force  $F$  is applied at  $z = 0$ , the free end of the beam, where the bending moment vanishes. The boundary conditions at  $z = 0$  are therefore given as

$$\phi'(0) = 0, \quad (\text{A6})$$

$$u'(0) - \phi(0) = -F/GA \kappa. \quad (\text{A7})$$

Assuming  $u = Ue^{sz}$  and  $\phi = \Phi e^{sz}$  and substituting them into equations (A2) and (A4) results in

$$\begin{bmatrix} k_f - \rho A \omega^2 - GA \kappa s^2 & GA \kappa s \\ -GA \kappa s & GA \kappa - \rho I \omega^2 - EI s^2 \end{bmatrix} \begin{Bmatrix} U \\ \Phi \end{Bmatrix} = \mathbf{0}. \quad (\text{A8})$$

The equation for  $s$  in terms of  $\omega$  can be found by equating to zero the determinant of the resultant matrix in (A8). Since damping is introduced by loss factors,  $s$  appears in two groups of complex values. One group is for wave propagation in the positive direction and the other in the negative direction. Supposing  $s = k_1, k_2$  belongs to the group for propagation in the positive direction, then the vertical displacement  $u$  and rotation  $\phi$  can be given as

$$u = A_1 e^{k_1 z} + A_2 e^{k_2 z}, \quad (\text{A9})$$

$$\phi = C_1 e^{k_1 z} + C_2 e^{k_2 z}. \quad (\text{A10})$$

$C_1$  can be found in terms of  $A_1$ , and  $C_2$  in terms of  $A_2$  by making use of either of the pairs of equations (A8). This yields

$$C_1 = A_1 \frac{k_1 G A \kappa}{G A \kappa - \rho I \omega^2 - k_1^2 E I}, \quad (\text{A11})$$

$$C_2 = A_2 \frac{k_2 G A \kappa}{G A \kappa - \rho I \omega^2 - k_2^2 E I}. \quad (\text{A12})$$

The boundary conditions described in equations (A6) and (A7) should be satisfied and this leads to the solutions for  $A_1$  and  $A_2$ :

$$A_1 = \frac{F/G A \kappa}{b_1(1 - k_1/k_2) - k_1(1 - b_1/b_2)}, \quad (\text{A13})$$

$$A_2 = \frac{F/G A \kappa}{b_2(1 - k_2/k_1) - k_2(1 - b_2/b_1)}, \quad (\text{A14})$$

where

$$b_1 = \frac{k_1 G A \kappa}{G A \kappa - \rho I \omega^2 - k_1^2 E I}, \quad (\text{A15})$$

$$b_2 = \frac{k_2 G A \kappa}{G A \kappa - \rho I \omega^2 - k_2^2 E I}. \quad (\text{A16})$$

The point receptance of the track at a rail joint is therefore given as

$$\alpha^R = \frac{u(0)}{2F} = \frac{A_1 + A_2}{2F}. \quad (\text{A17})$$

Here a factor of 1/2 is applied because it is assumed that only half the excitation is received by each of the rails at the joint where the force  $F$  acts.